Soft Matter

Design Rules for Encapsulating Proteins into Complex Coacervates

Journal:	*Soft Matter*
Manuscript ID	SM-ART-02-2019-000372.R1
Article Type:	Paper
Date Submitted by the Author:	15-Mar-2019
Complete List of Authors:	Blocher McTigue, Whitney; University of Massachusetts Amherst, Department of Chemical Engineering Perry, Sarah; University of Massachusetts Amherst, Department of Chemical Engineering; University of Massachusetts Amherst, Institute for Applied Life Sciences

Journal Name

ARTICLE

Design Rules for Encapsulating Proteins into Complex Coacervates

Whitney C. Blocher McTigue[a] and Sarah L. Perry[a]*

Received 00th January 20xx,
Accepted 00th January 20xx

DOI: 10.1039/x0xx00000x

www.rsc.org/

We investigated the encapsulation of the model proteins bovine serum albumin (BSA), human hemoglobin (Hb), and hen egg white lysozyme (HEWL) into two-polymer complex coacervates as a function of polymer and solution conditions. Electrostatic parameters such as pH, protein net charge, salt concentration, and polymer charge density can be used to modulate protein uptake. While the use of a two-polymer coacervation system enables the encapsulation of weakly charged proteins that would otherwise require chemical modification to facilitate electrostatic complexation, we observed significantly higher uptake for proteins whose structure includes a cluster of like-charged residues on the protein surface. In addition to enhancing uptake, the presence of a charge patch also increased the sensitivity of the system to modulation by other parameters, including the length of the complexing polymers. Lastly, our results suggest that the distribution of charge on a protein surface may lead to different scaling behaviour for both the encapsulation efficiency and partition coefficient as a function of the absolute difference between the protein isoelectric point and the solution pH. These results provide insight into possible biophysical mechanisms whereby cells can control the uptake of proteins into coacervate-like granules, and suggest future utility in applications ranging from medicine and sensing to remediation and biocatalysis.

Introduction

The encapsulation of proteins and other biomacromolecules is an area of accelerating activity, as such materials are finding increasing utility in applications including drug delivery, environmental remediation, personal care products and biocatalysis. However, proteins tend to be sensitive to their environment, and typical methods used for encapsulation can decrease or even destroy the activity of these molecules. While polymeric materials have been increasingly used for the encapsulation of proteins, the preparation of most polymeric materials requires the use of organic solvents that can accelerate the denaturation and aggregation of protein cargos.[1] In contrast, we examine the use of polymer-based complex coacervation as a gentle and fully aqueous strategy for achieving high levels of protein encapsulation.

Complex coacervation is an associative, liquid-liquid phase separation phenomenon driven by an initial electrostatic attraction between oppositely charged macroions[2-13] such as polymers,[14-20] surfactant micelles,[21-28] and colloids,[29] followed by entropic gains associated with the release of small, bound counter-ions and the restructuring of water.[2-5] The utility of complex coacervation as an encapsulation strategy has been highlighted, particularly in the areas of food science,[30,31] personal care products,[32,33] and medicine,[34] because of the ability to generate formulations and drive encapsulation without the need of organic solvents.[5,7,35,36]

One potential limitation of complex coacervation is its reliance on electrostatic interactions to facilitate protein encapsulation. Due to the fact that protein molecules contain numerous charged groups, their net charge is a convolution of composition and solution conditions. In particular, Obermeyer and co-workers demonstrated that a threshold level of net charge is needed to enable coacervation of proteins with an oppositely-charged polymer.[8,37,38] Thus, while methods such as chemical ligation or point mutations could be used to modify the net charge of a protein, there are numerous targets that might be inaccessible to such a coacervation-based approach because of their charge profile. In contrast, work by Tirrell and co-workers demonstrated the ability to achieve high levels of protein encapsulation through the use of a ternary system where the protein of interest is complexed with a mixture of cationic and anionic polymers.[7] Furthermore, work by the same group showed that coacervates formed from a ternary system of polyelectrolytes showed complexation over a broader range of polymer compositions than would be expected for the individual binary systems.[39]

We hypothesize that the use of a two-polymer system should increase the robustness of protein encapsulation via complex coacervation, and that tailoring of the presentation of charges on the polymers, in addition to the solution conditions, can further enhance protein encapsulation. This hypothesis is inspired by increasing reports of liquid-liquid phase separated

[a] Department of Chemical Engineering and the Institute for Applied Life Sciences, University of Massachusetts Amherst, Amherst, MA 01003 USA.
Email: perrys@engin.umass.edu

Electronic Supplementary Information (ESI) available: Tables of physical parameters for proteins and polymers, additional plots of turbidity, protein concentration, protein encapsulation efficiency and partition coefficient, and code for the calculation of pI and g(r). See DOI: 10.1039/x0xx00000x

Journal Name

ARTICLE

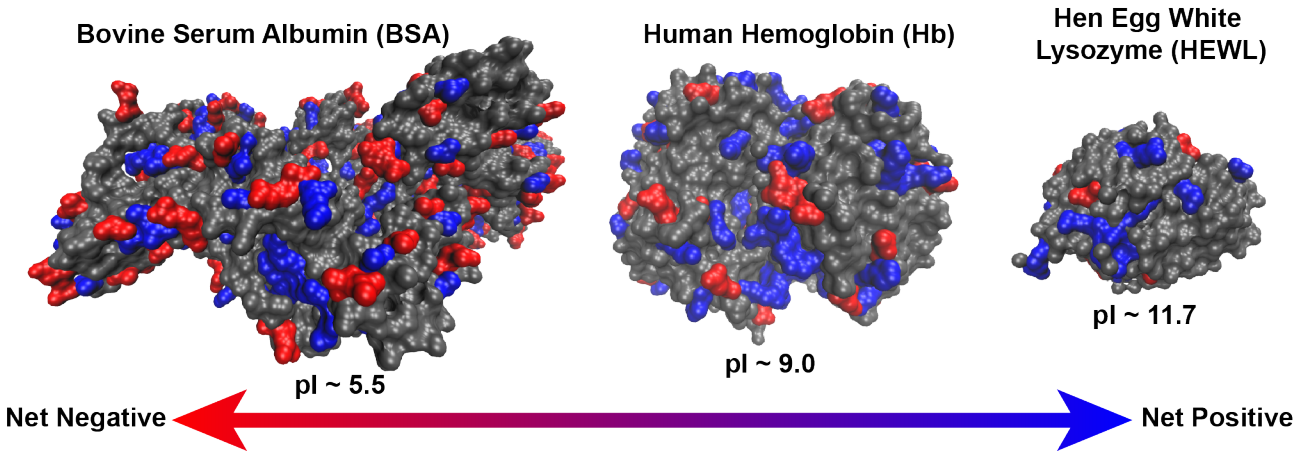

Figure 1. Structural rendering of the model proteins bovine serum albumin (BSA), the tetrameric form of human hemoglobin (Hb), and hen egg white lysozyme (HEWL) highlighting the location and distribution of charged residues. Negatively-charged glutamate and aspartate residues are shown in red. Positively-charged histidine, lysine, and arginine are shown in blue. The listed isoelectric point (pI) was obtained from theoretical calculations based on the Henderson-Hasselbalch equation.

biomolecular condensates in cells, also referred to as membraneless organelles.[40-51] These compartments are typically formed from a mixture of intrinsically disordered proteins and RNA, some of which have been shown to form via complex coacervation.[52-54] Most relevant to our hypothesis is evidence from the study of stress granules where the specific materials that drive phase separation are also able to selectively incorporate enzymes related to the triggering signal.[55-61] These encapsulated proteins can be held in storage at high concentrations while maintaining their stability.[62] This ability to selectively encapsulate and concentrate specific proteins from solution suggests that such bio-inspired coacervation could be used to enable a wide range of applications.

In this report we utilized bovine serum albumin (BSA), human hemoglobin (Hb), and hen egg white lysozyme (HEWL) as model proteins that cover a range of charge profiles and protein sizes (Figure 1). We incorporated these proteins into a two-polymer coacervate system composed of poly(*L*-lysine) (K_n) and poly(*D,L*-glutamate) (E_n) to enable the exploration of molecular-level design rules for protein encapsulation as a function of protein characteristics, as well as pH, ionic strength, polymer length, and polymer charge density.

Materials and Methods

Materials

Bovine serum albumin (BSA) (≥98%) and human hemoglobin (Hb) were purchased from Sigma Aldrich as lyophilized powders. Hen egg white lysozyme (HEWL) (≥95%) was purchased from Hampton Research as a lyophilized powder. The zwitterionic buffers 2-(*N*-morpholino)ethanesulfonic acid (MES) (≥98%) and (4-(2-hydroxyethyl)-1-piperazineethanesulfonic acid) (HEPES) (≥99%) were purchased as powders from Fisher Scientific. A monoclonal antibody (mAb) was a gift from MassBiologics.

Poly(*L*-lysine trifluoroacetate) and poly(*D,L*-glutamate sodium salt) with a degree of polymerization of N = 50 (K_{50}, E_{50}) were made in-house via solid-phase synthesis.[63] In particular, E_{50} was synthesized using amino acids of alternating chirality (*D* and *L*). Poly(*L*-lysine trifluoroacetate or bromide) and racemic poly(*D,L*-glutamate sodium salt) with chain lengths of 100, 400, and 800 were purchased from Alamanda Polymers and used without further purification. See Table S1 for more information related to the polymers. Poly(*D,L*-glutamate) (E_n) was used in all experiments in order to prevent the formation of hydrogen bonds between complexing chains of K_n and E_n chains that would result in solid precipitation rather than liquid complex coacervation.[4,6,64]

Peptide Synthesis

Polypeptides with N = 50 were prepared using standard Fmoc-based solid-phase synthesis[63] on a Liberty Blue automated microwave peptide synthesizer from CEM, Ltd. as previously reported.[65] Briefly, polypeptides were prepared on a Rink amide MBHA resin (Peptide Solutions) using (Fmoc-*L*-Lys(Boc)-OH, (Fmoc-*L*-Glu(tBu)-OH, and Fmoc-*D*-Glu(tBu)-OH (Peptide Solutions). 20% piperidine (Sigma Aldrich) in N,N-dimethylformamide (DMF, sequencing grade, Fisher BioReagents) was used for Fmoc deprotection. 0.5M N,N-diisopropylcarbodiimide (DIC, 99% Acros Organics) and 1M

ethyl (hydroxyimino)cyanoacetate (Oxyma, Peptide Solutions) in DMF were used as activator and base, respectively. Cleavage of the polypeptide from the resin and side-chain deprotection was performed using trifluoroacetic acid (TFA, Fisher)/water (MilliQ 18.2 MΩ.cm, Millipore)/triisopropylsilane (TIPS, 98% Acros Organics) in the ratio of 95/2.5/2.5 for 3 hours at room temperature while bubbling with carbon dioxide. The crude polypeptide was then precipitated into cold (stored at -80°C) anhydrous ethyl ether (BHT stabilized, Fisher Scientific). Characterization of the final product was performed via a Bruker UltrafleXtreme (Fremont, CA, USA) matrix-assisted laser desorption/ionization time of flight mass spectrometer (MALDI-TOF).

Preparation of Stock Solutions

Stock solutions of 10 mM polypeptide (*i.e.*, polymer) were prepared gravimetrically in Milli-Q water and adjusted to the desired pH ±0.03 pH units (Thermo Scientific ROSS Sure-Flow Combination pH) with 1 M HCl and 1 M NaOH. 0.5 M MES buffer was prepared at pH 6.0 and solutions of 0.5 M HEPES buffer were prepared at pH 7.0 and 8.0. Stock solutions of 2.0 mg/mL protein, BSA (0.030 mM), HEWL (0.14 mM), and Hb (0.031 mM), were similarly prepared in 10 mM buffer at the relevant pH. The solution pH was further adjusted to within ±0.03 pH units of the desired pH, if needed. The protein solutions were then separated into 105 µL aliquots and stored at -20°C until use to minimize the potential for adverse effects from multiple freeze-thaw cycles. Sodium chloride (NaCl) was purchased from Sigma Aldrich (≥99%) and stock solutions were made at both 2 M and 0.5 M NaCl and pH adjusted as above.

Coacervate Formation

Coacervate samples were prepared by first pipetting water, buffer and then salt (as needed) into a 1.5 mL microcentrifuge tube (Fisher Scientific), followed by the protein and one of the polymers. Preliminary experiments suggested that the order of polymer addition did not significantly affect the outcome (Figure S1). Thus the order of addition for HEWL was protein, followed by E_n and K_n, while for BSA and Hb the order of addition was protein, followed by K_n and E_n. The samples were then vortexed to facilitate mixing before addition of the second polymer, and were then vortexed immediately after pipetting to ensure fast and complete mixing. A typical experiment varied the ratio of K_n to E_n over 15 samples at a total monomer concentration of 7 mM for the polymer species (on a monomer basis) while maintaining a constant protein concentration of 50 µg/mL. Each sample contained a total volume of 240 µL, 105 µL of which was used for turbidimetric analysis, with the remaining 135 µL used for quantification of protein encapsulation. All experiments were performed in triplicate.

Turbidimetry and Optical Microscopy

Following sample preparation, three 35 µL replicate aliquots of each sample were pipetted into a 384-well plate (Falcon). Turbidity measurements were performed in triplicate using a microplate reader (BioTek Synergy H1) at a wavelength of 562 nm. Turbidity is defined as $-\ln(I/I_0)$, where I_0 = incident light intensity and I = intensity of the light passed through the sample, and is measured in absorbance units (a.u.). The measured signal was referenced against a well containing water, buffer, and salt (if present). Samples were then inspected using optical microscopy (EVOS XL Core) to confirm the presence or absence of coacervation.

Quantifying Protein Encapsulation and Partitioning

The colorimetric Bradford assay was used to quantify the amount of protein present in both the coacervate and supernatant of each sample.[7] The 135 µL of sample remaining in the microcentrifuge tube after turbidimetric analysis was centrifuged (Thermo Scientific Sorvall Legend Micro 21R Centrifuge) at 14,000 rpm (18.8×g) for 20 min and 15°C. Following centrifugation, the supernatant was carefully removed, and the volume of supernatant was measured via pipetting. From the total volume of supernatant, 115 µL was transferred into a new microcentrifuge tube. 70 µL of 2 M NaCl was added to the original microcentrifuge tube to disassemble any coalesced coacervate that might be present, followed by vortexing. We estimated that the maximum volume of coacervate formed was on the order of ~1-2 µL. However, because of the difficulty in quantifying such a small volume, the volume of the coacervate was neglected in the subsequent concentration calculations. Coomassie Plus™ protein assay reagent (Thermo Scientific) was then added to both the coacervate and supernatant samples and mixed by vortexing. The quantity of dye added to the various samples was adjusted based on the amount of protein present. For BSA- and Hb-containing samples, a 1:1 volumetric ratio of Coomassie dye was added to both the supernatant (115 µL of dye) and coacervate (70 µL of dye). For HEWL-containing samples, a 2:1 volumetric ratio of dye-to-sample was used for supernatant-containing samples (230 µL of dye), while a 1:1 volumetric ratio of dye-to-sample was used for the coacervate samples (70 µL of dye).

Protein concentration was quantified via UV-Vis analysis using a microplate reader (BioTek Synergy H1). Three aliquots of 35 µL for each sample were pipetted into a 384-well plate and read at 595 nm in triplicate. Calibration curves for each protein were generated using the same buffer and salt conditions, as well as the same dye-to-sample ratio, to determine the concentration of protein in both the supernatant and coacervate phases. These concentrations were used directly to calculate the partition coefficient between the coacervate and the supernatant phases after a baseline subtraction. The partition coefficient (K, Eq. 1) was defined as the ratio of the concentration of protein in the coacervate divided by the concentration of protein in the supernatant.

$$K = \frac{C_{protein\ in\ coacervate}}{C_{protein\ in\ supernatnat}} \quad (1)$$

Baseline correction of the measured concentration of protein in the coacervate phase was necessary in order to account for residual protein bound to the surface of the microcentrifuge tube. Turbidity measurements and visual inspection confirmed that phase separation was not observed for samples at the extremes of the stoichiometric range (0.1 and 0.9 mole fraction polycation, Figure 2 and Figures S3, S5, S9, and S13).

Thus, a baseline subtraction was performed using the measured absorbance values at 0.1 and 0.9 mole fraction from the "coacervate" tube to correct for this contamination. Such adjustment was only necessary for the coacervate phase, as the small volumes and high viscosity of the material did not allow for effective transfer to a clean microcentrifuge tube for quantification.

A mass balance on the system was used to determine the mass of protein in each phase. The mass of protein in the coacervate phase was calculated as the difference between the total mass of protein added and the mass of protein in the supernatant. This approach was used because of the challenges associated with accurately measuring coacervate volumes on the order of 1-2 µL or less. Encapsulation efficiency (EE%, Eq. 2) was defined as the mass of protein in the coacervate (determined via mass balance) relative to the total mass of protein in the system.

$$EE\% = \frac{m_{total} - m_{supernatant}}{m_{total}} \text{x} 100\% \quad (2)$$

Determination of Net Charge and Isoelectric Point

The net charge and isoelectric point (pI) for each protein was calculated as a function of pH using a MATLAB (Mathworks Inc.) script based on the Henderson-Hasselbalch equation. Graphs of the protein charge as a function of pH (Figure S2), the calculated values for the net charge (Table S2), total number of charges (Table S3), and pI (Table S4), as well as the full code are available in the Supplementary Information. The calculated values for the pI for BSA[66-69] and HEWL[66,70] match well with experimentally reported values from the literature. A wide range of pI values have been reported for Hb,[71-74] because it is composed of two chains (α,β) that assemble as a pair and then as a tetramer.

Calculation of the Radial Distribution Function for Charged Residues

A second MATLAB code was used to calculate the radial distribution function $g(r)$, also known as a pair correlation function, between charged residues to identify the presence of charge patches on the protein surface. Briefly, the three-dimensional coordinates for a protein structure were first extracted from a PDB[75] file and read into MATLAB. The spatial coordinates of the α-carbon of aspartate (D), glutamate (E), lysine (K), histidine (H), and arginine (R) residues were then extracted and used in the calculation of $g(r)$. This calculation did not take into account pH effects or the potential for local differences in the charge state of the various residues. The radial distribution was then calculated using each of the residues in turn. Integration was performed using a 2 Å step over a total distance of 50 Å. The data were then plotted as a function of charged residue and radius. The following PDB structures were used in this calculation: 3V03 for BSA,[76] 2DN1 for Hb (considering a single pair of α/β chains, rather than the full tetrameric biological assembly),[77] and 1DPX for HEWL.[78] The full code is available in the Supplementary Information.

Statistical Analysis

Statistical analysis was performed using an unpaired, two-tailed Student's t test. An asterisk (∗) denotes $p < 0.05$ between samples. The error bars shown on all graphs represent the propagated standard deviation determined from the variation in repeated experiments convoluted with the uncertainty in the various calibration curves and relevant calculations.

Results and Discussion

The goal of this work is to establish a rational framework for understanding the uptake and encapsulation of globular proteins into complex coacervate systems. While recent studies showed that protein net charge is critical for the formation of complex coacervates in binary protein/polymer systems,[8,37,38] our work focused on the potential for expanding the range of conditions over which proteins can be incorporated into such materials. In particular, our approach takes advantage of ternary coacervates that contain both a polyanion and a polycation, in addition to the protein.

Here, we examined the coacervation of three model proteins, bovine serum albumin (BSA), human hemoglobin (Hb), and hen egg white lysozyme (HEWL), with a two-polymer coacervate system composed of poly(*L*-lysine) (K_n) and poly(*D,L*-glutamate) (E_n). These proteins were chosen as they represent a range of molecular weights and net charges (Figure 1). BSA has a calculated pI ~ 5.5, and thus would be expected to have a net negative charge at the solution conditions studied here. In contrast, Hb has a pI ~ 9.0 and HEWL has a pI ~ 11.7, and would be expected to be net positive at the conditions studied here. With respect to size, both BSA and Hb are approximately three times larger than HEWL, but have differing numbers of charged residues, allowing for a more nuanced comparison of the effects of size and charge (Table S4).

Protein Encapsulation as a Function of Coacervate Charge Stoichiometry

Turbidity was used as a qualitative measure of the presence of phase separation in a sample. We first performed an initial characterization looking at how the presence of protein in our sample affected the conditions at which complex coacervation occurs. For the simple case of a binary system where both polymers are fully charged and no added salt was present, we observed a turbidity peak centred at a mole fraction of 0.5 (polycation relative to the total polymer concentration).[2,79,80] This result highlights the electrostatic nature of complex coacervation, and the preference for the system to reach charge neutrality. When a charged protein was added as a third component, we observed a slight broadening in the range of charge ratios over which coacervation was observed (Figures 2a,c,e, and Figures S3, S5, S9, S13), suggesting the presence of more synergistic interactions.[39] Generally speaking, we observed shifts in the turbidity commensurate with the charge of the added protein. For negatively charged BSA at pH 7.0, we observed a small shift in the maximum

Journal Name

ARTICLE

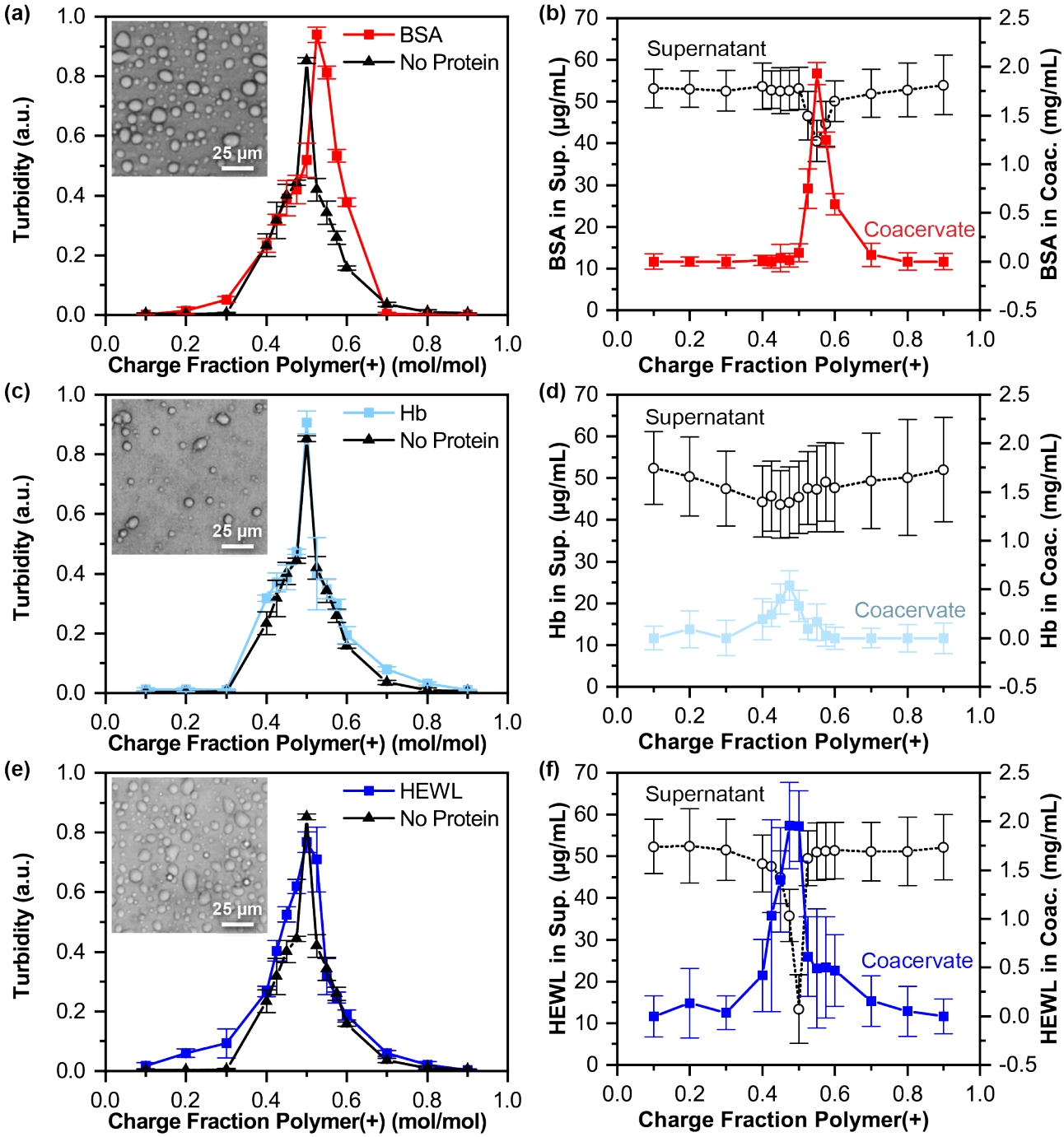

Figure 2. Plots of turbidity as a function of the charge fraction of the polycation for coacervates of K_{50} and E_{50} in the presence and absence of **(a)** BSA, **(c)** Hb, and **(e)** HEWL in 10 mM HEPES, pH 7.0. The inset optical micrographs show the liquid coacervate droplets formed at the peak in turbidity for the system. The corresponding plots of protein concentration in the supernatant (dashed black) and coacervate (solid) as a function of the charge fraction of the polycation for **(b)** BSA, **(d)** Hb, and **(f)** HEWL. A decrease in protein concentration in the supernatant phase is matched by an increase in the protein concentration in the coacervate phase over the range of mole fractions indicated by turbidity. Lines connecting data points are a guide to the eye. Error bars are the standard deviation of the reported average, including propagated error.

Journal Name

ARTICLE

turbidity to higher mole fractions of K (Figure 2a). This shift means that more cationic K_{50} was needed to achieve a charge neutral coacervate. The opposite trend was observed for positively charged HEWL, where we observed a shift in the turbidity to lower mole fractions of K_{50} (Figure 2e), indicating that more anionic E_{50} was needed to balance out the combined cationic charge of both K_{50} and HEWL. There was little shifting for Hb, presumably due to the low net charge of the protein at pH 7.0.

While turbidity, coupled with visual inspection and optical microscopy allowed for a determination of the range of conditions over which coacervation occurs, it did not provide a direct indication of whether or not the protein was taken up into the coacervate. Thus, we coupled our turbidimetric studies with a colorimetric Bradford assay to quantify the concentration of protein in both the supernatant and coacervate phases.

The Coomassie Brilliant Blue G-250 dye used in the Bradford assay enables protein quantification via binding with basic residues. However, this binding is enhanced by van der Waals forces and hydrophobic interactions, which would be present in a folded protein, but less so in our polypeptide-based polymers.[81] Analysis of the interaction between the Coomassie dye and our coacervate materials showed that the pairing between oppositely-charged polymers in the coacervate resulted in negligible signal (Figure S17). For the supernatant, we observed a relatively constant baseline signal for all polymer ratios where phase separation was not observed, and negligible signal when phase separation occurred. Data analysis demonstrated that our measurements and approach were able to recapitulate the starting concentration of protein in the supernatant for samples where phase separation was not observed (within error). Furthermore, we observed the correlated uptake of protein into the coacervate phase and depletion of protein from the supernatant when phase separation did occur, and where background signal from the polymers is expected to be minimal (Figure 2b,d,f, and Figures S4, S6-8, S10-12, S14-16). For example, Figure 2b shows that at low cationic charge fractions, the amount of BSA in the supernatant was not significantly different from the starting concentration of 50 µg/mL, but at cationic charge fractions near 0.5 where phase separation was observed (*i.e.*, net neutrality), BSA favoured uptake into the coacervate phase, resulting in a strong increase in the concentration of BSA in the coacervate and a commensurate decrease of protein in the supernatant. At higher charge fractions, phase separation was

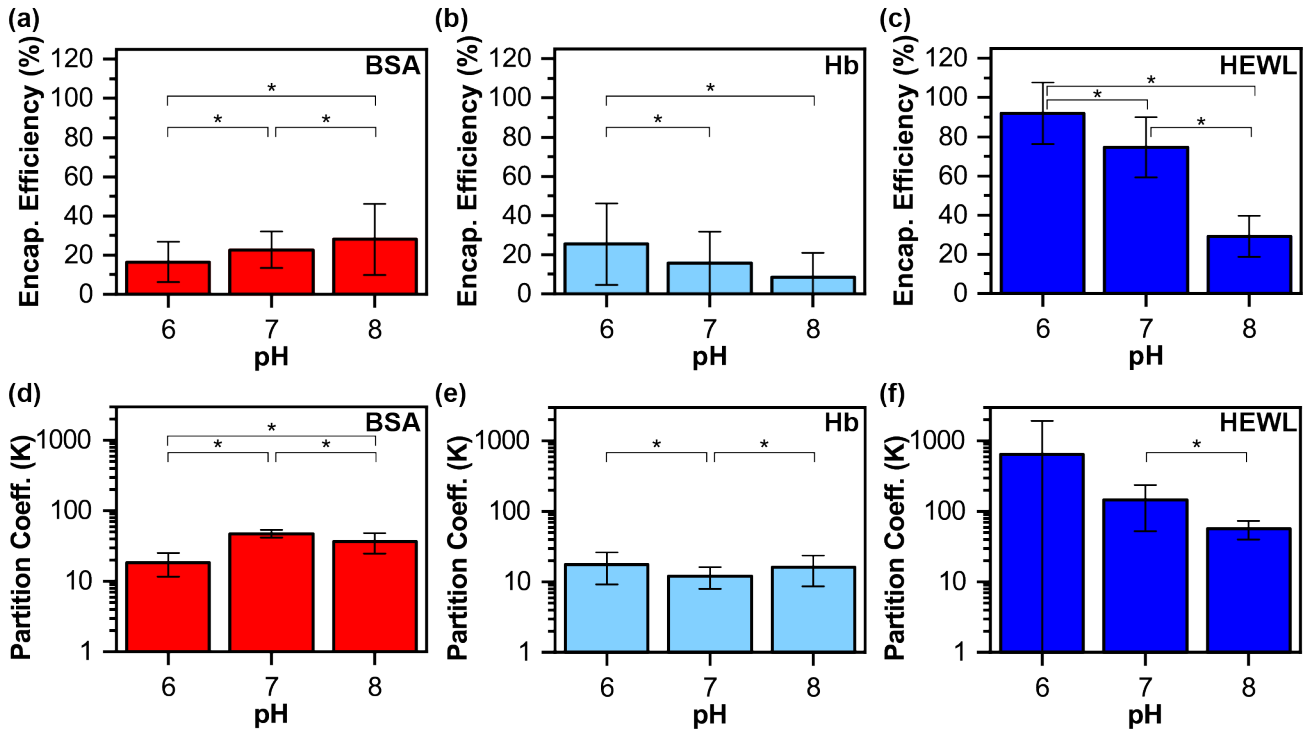

Figure 3. Plots of maximum encapsulation efficiency **(a-c)** and maximum partition coefficient **(d-f)** as a function of solution pH for BSA (red, pI = 5.5), Hb (light blue, pI = 9.0), and HEWL (dark blue, pI = 11.7), respectively. Coacervates were prepared using N = 50 polymers with no added salt and 10 mM buffer. An asterisk (∗) denotes $p < 0.05$, and error bars are the standard deviation of the reported average, including propagated error.

Journal Name

ARTICLE

again disfavoured, and the protein preferentially returned to the initial levels in the supernatant. Similar results were observed for the other two proteins, although a much lower change in concentration was observed for Hb (Figure 2 and Figures S4, S6-8, S10-12, S14-16). Interestingly, the maximum concentration in the dense phase, as well as the minimum concentration in the dilute phase, occurred around the same point as the maximum in the turbidity readings. Thus, while turbidity is not a necessary indicator of encapsulation, it may prove to be sufficient in many cases.

pH Dependence

Prior reports, as well as the results in Figure 2 have highlighted the key role that electrostatics plays in driving protein encapsulation via complex coacervation.[8,37,38,51,82-86] To further explore this, we examined how changing the solution pH and thus the charge of the protein affected encapsulation. There are numerous ways of describing the charge state of a protein, including explicitly counting the number of charges. However, we used the isoelectric point (pI) as a general, qualitative indicator of the protein charge state. The pI describes the solution pH where a protein has an equal number of positive and negative charges. Thus, for solution conditions where the pH is lower than the pI, the protein would have a net positive charge, whereas if the solution pH were higher than the pI, the protein would have a net negative charge. The farther the pH is from the pI, the higher the absolute value of the net charge, up to a limit.

We performed experiments at three different solution pH conditions of 6.0, 7.0, and 8.0. Across these pH values, we expected to modulate the charge state of our proteins due to titration of the histidine residues (Figure S2 and Tables S2, S3). This range of pH values was chosen specifically to minimize pH effects on the degree of ionization of our charged polymers such that the calculated change would be less than 10% (Figure S2d,e and Table S2).

Experimentally, as the pH was increased from 6.0 to 8.0, moving away from the theoretical pI for BSA of 5.5, we observed an increase in both encapsulation efficiency and partitioning (Figure 3a,d and Figure S4a,b). A similar trend was observed for Hb (Figure 3b,e and Figure S4c,d) and HEWL (Figure 3c,f and Figure S4e,f) as the pH was decreased from 8.0 to 6.0, moving away from the theoretical pI for these proteins of 9.0 and 11.7, respectively. While these trends matched our intuition regarding the importance of electrostatics in driving

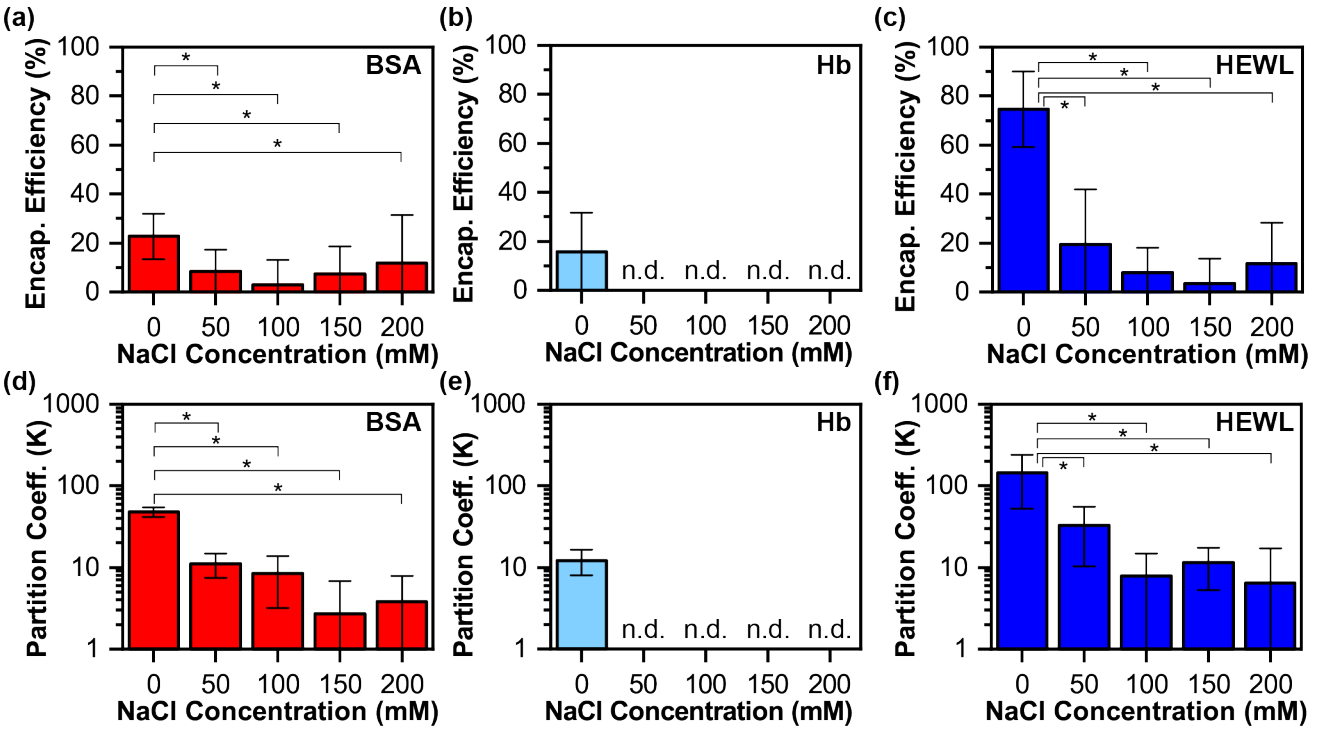

Figure 4. Plots of maximum encapsulation efficiency **(a-c)** and maximum partition coefficient **(d-f)** as a function of the as-prepared salt concentration for BSA (red), Hb (light blue), and HEWL (dark blue), respectively. Coacervates were prepared using N = 50 polymers and 10 mM buffer, pH = 7.0. An asterisk (*) denotes $p < 0.05$, and error bars are the standard deviation of the reported average, including propagated error.

Journal Name

ARTICLE

protein encapsulation, we also observed significant quantitative differences with respect to the partitioning and levels of encapsulation efficiency achieved for each of the various proteins. In particular, we observed significantly higher levels of protein incorporation for HEWL-containing coacervates than for the BSA and Hb systems.

Salt Dependence

Salt concentration and/or ionic strength can also be an important parameter in terms of complex coacervation. We examined the effect of increasing NaCl concentrations (from 0 to 200 mM) on the uptake of protein into the coacervate phase. We observed a decrease in the partitioning of all three of our proteins into the coacervate phase with increasing salt concentration (Figure 4d-f and Figures S6-S8). We hypothesize that this decrease in protein concentration may be a result of a weakening of the electrostatic and entropic interactions that facilitate coacervation and inclusion of the less strongly charged protein in the presence of more strongly-charged polymer chains.[87] In particular, the addition of even 50 mM NaCl was sufficient to overcome the interactions favouring partitioning of the weakly charged Hb into the coacervate phase, such that no uptake could be measured in the presence of added salt (Figure 4e and Figure S7).

Interestingly, we observed a somewhat different trend for encapsulation efficiency. The encapsulation efficiency of BSA and HEWL showed a minimum in the range of 100-150 mM NaCl (Figure 4a,c). The apparent difference between the trends in partitioning and encapsulation efficiency relates to how the two descriptors vary as a function of coacervate volume. A partition coefficient is defined as the equilibrium ratio of concentrations between two phases, and should remain constant regardless of the volume of the two phases. In contrast, encapsulation efficiency quantifies the absolute amount of protein that has been taken up into the coacervate phase. Thus, for a system with the same relative concentrations of protein in the coacervate and supernatant phases, increasing the volume of the coacervate phase would result in an increase in encapsulation efficiency while leaving the partition coefficient unchanged. Thus, the difference in the salt dependent uptake of our various proteins is a consequence of how the presence of protein and salt affects both the electrostatic interactions driving uptake and the total coacervate volume.[88-90]

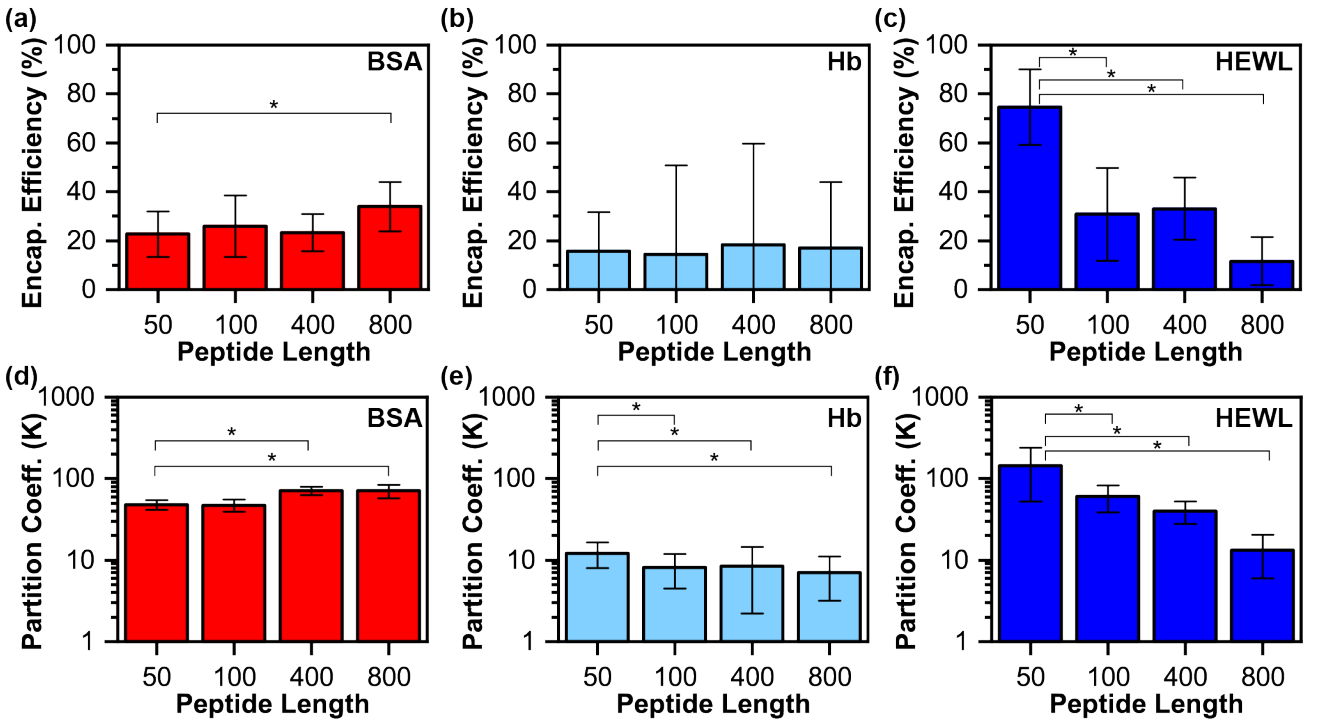

Figure 5. Plots of maximum encapsulation efficiency **(a-c)** and maximum partition coefficient **(d-f)** as a function of the degree of polymerization of the complexing polymers for BSA (red), Hb (light blue), and HEWL (dark blue), respectively. Coacervates were prepared with no added salt and 10 mM buffer, pH = 7.0. An asterisk (*) denotes $p < 0.05$, and error bars are the standard deviation of the reported average, including propagated error.

Journal Name

ARTICLE

While the concentration of salt present in the formulation may serve as a potential parameter in tuning protein encapsulation, we acknowledge that salt concentration and/or ionic strength may be less flexible due to protein stability or other application-specific requirements. Furthermore, although we only investigated the effects of NaCl in the study, we would anticipate that salt valence and Hofmeister effects should similarly affect protein uptake based on literature reports on the effects of salt on coacervation more generally.[2,91-94]

Peptide Chain Length Dependence

To further investigate the competition between protein and polymer, we next examined the effect that polymer length has on the encapsulation of our model proteins using four different chain lengths polymers N = 50, 100, 400, 800. We hypothesize that longer polymer chains would compete with the more weakly charged protein in terms of complex formation, leading to a decrease in protein encapsulation with increasing chain length.[87] While we observed this type of behaviour for both the encapsulation efficiency and partitioning of HEWL (Figure 5c,f and Figure S12), a statistically significant decrease was only observed for the partitioning of Hb (Figure 5e and Figure S11). BSA showed very little variation in either encapsulation efficiency or partitioning as a function of polymer chain length (Figure 5a,c and Figure S10).

To explain these different trends in uptake, we investigated

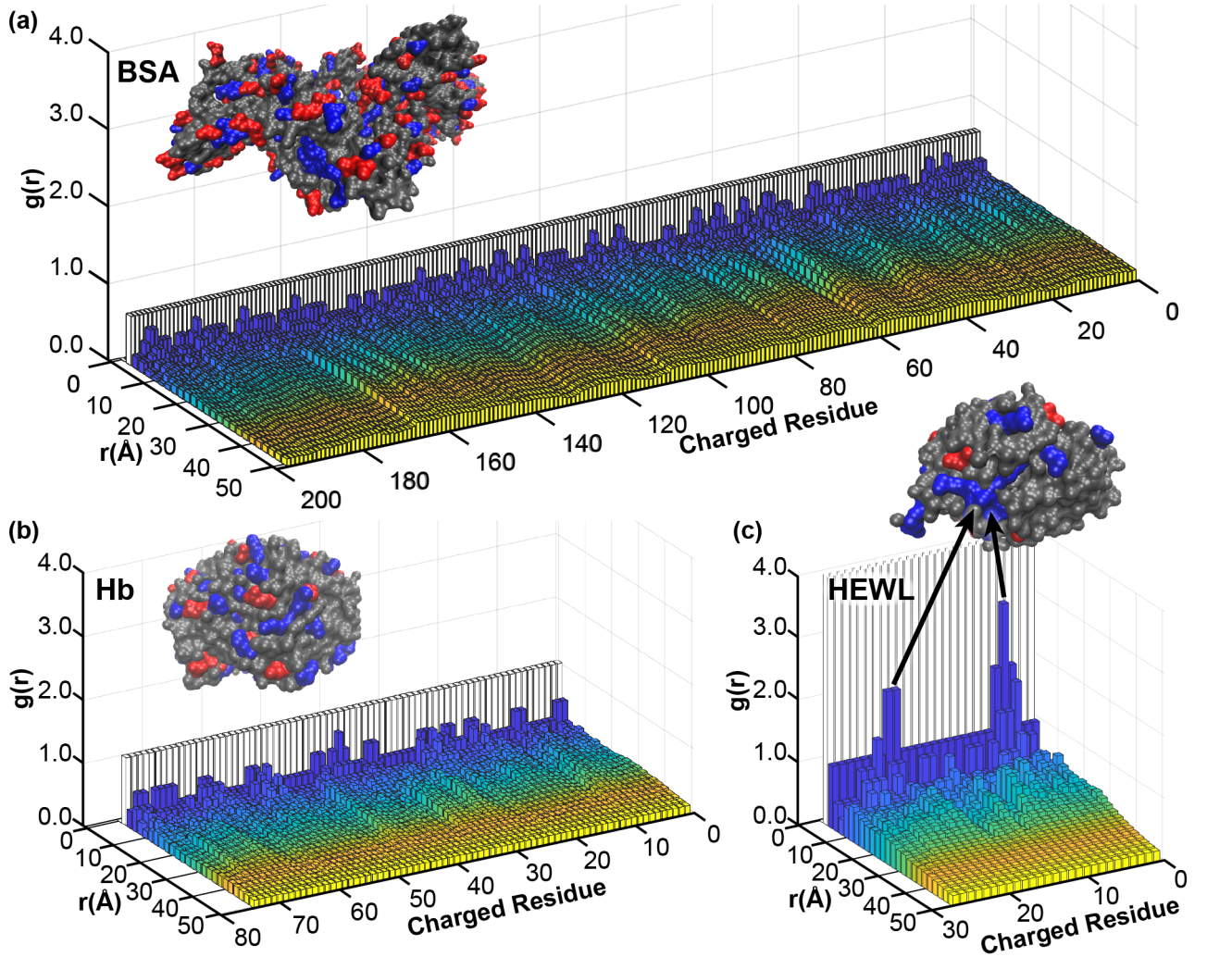

Figure 6. 3D bar plot depictions of the radial distribution function g(r) with respect to the charged amino acids in **(a)** BSA, **(b)** Hb, and **(c)** HEWL. The arrows in **(c)** indicate the residues associated with the identified charge patch. Protein structures are not shown at scale.

Journal Name

ARTICLE

whether size differences in our various proteins could account for our results.

HEWL is the smallest protein used in these experiments, with a molecular weight of 14.3 kDa (129 amino acids), while BSA and Hb are significantly larger with molecular weights of 66.4 kDa (583 amino acids) and 64.5 kDa (574 amino acids), respectively. Although we observed a significant drop in the uptake of HEWL when the polymer length approached the size of the protein (*i.e.*, going from N = 50 to N = 100), no similar change in uptake was observed going from N = 400 to N = 800. Similarly, the number of charged residues in the protein (Table S4) was also not a predictor of protein encapsulation. Thus, we hypothesize that the observed differences in protein encapsulation as a function of polymer chain length may be less a consequence of the number of charges, but more a function of the arrangement, or clustering of charges on the protein surface.

Charge Patchiness

To quantify potential charge clusters within a protein structure, we determined the radial distribution function $g(r)$ between all of the charged residues in each of our proteins (Figure 6 and S18). Interestingly, we only observed evidence of charge clustering for the case of HEWL, which had shown both the highest overall uptake, and significant length-dependent encapsulation effects (Figure 6c). In contrast, the $g(r)$ analysis of both BSA and Hb showed only the presence of medium-range correlations at length scales characteristic of the overall protein size. Thus, we hypothesize that the diffuse arrangement of charges on the surfaces of BSA and Hb means that complexation and uptake into the coacervate phase is dominated by promiscuous electrostatic interactions with numerous polymer chains, rather than a strong binary interaction between a charge patch and a single polymer chain for which length-dependent competition might be relevant.[87] Our hypothesis is supported by recent work by Kapelner and Obermeyer, who demonstrated that coacervates formed by a cationic polymer and a variant of green fluorescent protein (GFP) containing an anionic protein tag were significantly more stable than coacervates formed using mutants with the same net charge distributed isotropically on the protein surface.[38] These results may also be relevant from an evolutionary standpoint, in that it would most likely be disadvantageous for

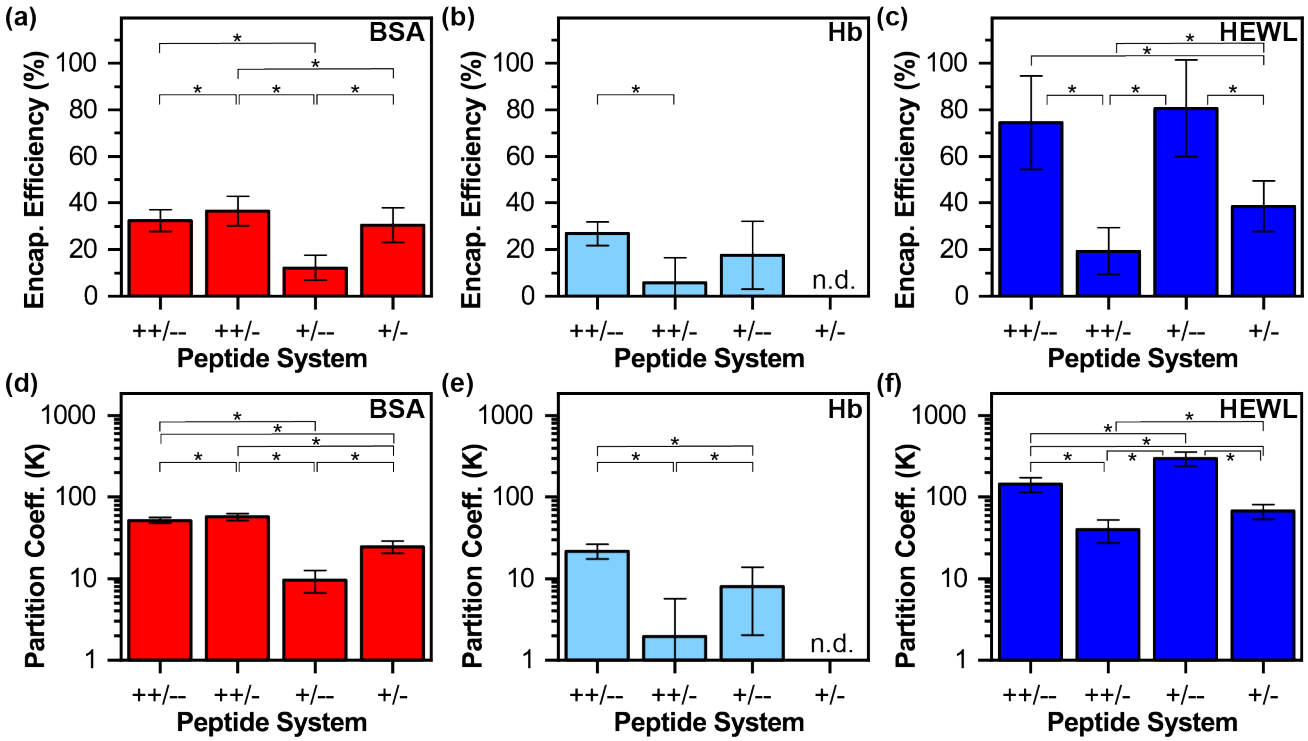

Figure 7. Plots of maximum encapsulation efficiency **(a-c)** and maximum partition coefficient **(d-f)** as a function of the level of charge content and/or patterning of the complexing polymer for BSA (red), Hb (light blue), and HEWL (dark blue), respectively. The polymer systems are denoted: K_{50}/E_{50} as ++/--, $K_{50}/(EG)_{25}$ as ++/-, $(KG)_{25}/E_{50}$ as +/--, and $(KG)_{25}/(EG)_{25}$ as +/-. Coacervates were prepared with no added salt and 10 mM buffer, pH = 7.0. An asterisk (*) denotes $p < 0.05$, and error bars are the standard deviation of the reported average, including propagated error.

Journal Name

ARTICLE

proteins such as BSA and Hb that are naturally present at high concentrations to interact strongly with other biomacromolecules. While the role of BSA and Hb does not require binding to other macromolecular species, HEWL functions to bind to and destroy bacteria. Thus, HEWL has evolved to have a positive charge patch to facilitate binding to the negatively charged surfaces of bacteria.[95-97] As such, understanding how different arrangements of charge on a protein affect encapsulation may lead to relevant insights for both biological processes and industrial applications including encapsulation and purification.[79,98]

Polymer Patterning and Charge Density

We further explored the impact of charge patchiness by considering the effect of the charge density of the coacervating polymers. In addition to the results already presented using homopolymer lysine and glutamate systems, we systematically substituted one or both of the charged homopolymers for a sequence-controlled copolymer where half of the charged residues were replaced by neutral glycine monomers.

Based on our understanding of the importance of electrostatic interactions on protein uptake, we expected to see enhanced partitioning when the homopolymer with the same charge as the protein was substituted for a less charged copolymer, and a decrease in partitioning when the oppositely-charged polymer was substituted for the lower charge density copolymer. We observed these outcomes for both partitioning and encapsulation efficiency for all of our proteins (Figure 7 and Figures S14-16). In the case of Hb the decrease in electrostatic interactions when both polymers were half charged resulted in no detectable protein uptake. Further exploration of the effects of different charge patterned polymers is an intriguing question for further study.

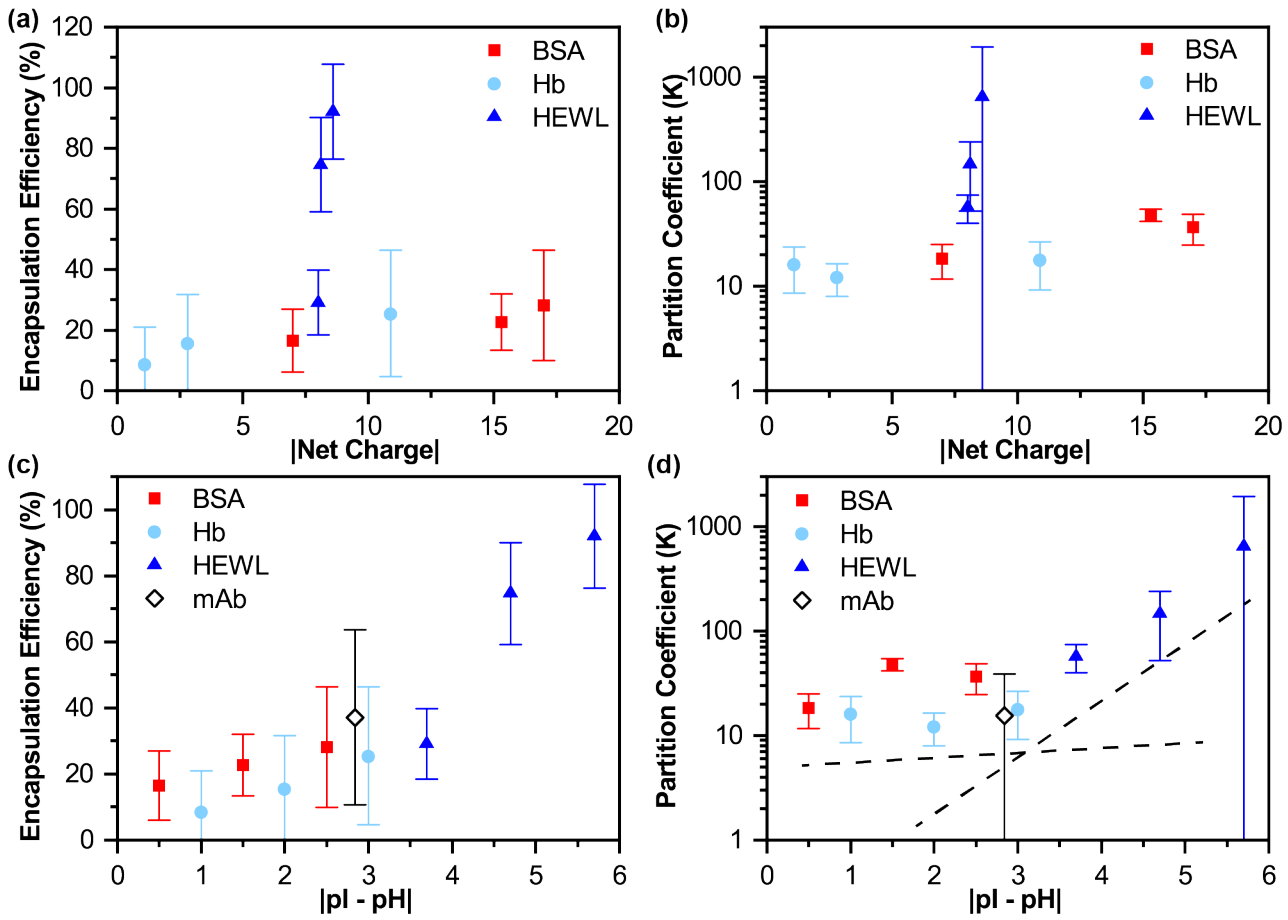

Figure 8. Plots of **(a)** maximum encapsulation efficiency and **(b)** maximum partition coefficient as a function of the absolute difference between the pI and pH and plots of **(c)** encapsulation efficiency and **(d)** partition coefficient as a function of absolute net charge. The dashed lines are guides for slopes for two different regimes. Coacervates were prepared using N = 50 polymers with no added salt and 10 mM buffer. Error bars are the standard deviation of the reported average, including propagated error.

Journal Name

ARTICLE

Correlating Physical Properties and Protein Encapsulation

While the results presented thus far have suggested the ways in which protein uptake may vary as a function of pH, salt concentration, polymer length, and polymer charge density, we still lack a general intuition on how the uptake of one protein might compare to another given the same set of solution conditions. To try and identify a physical property that might serve to guide estimations of the encapsulation potential of a novel protein system, we considered a number of different descriptors of the charge state of our system, including the relative distance from the isoelectric point $|pI - pH|$, the net charge of the protein, the net charge of the protein normalized by the total number of residues, and the ratio of positive to negative charges (Tables S2-S4, Figure 8 and Figure S19).

While each of these metrics might be expected to give similar results, the relative distance from the isoelectric point $|pI - pH|$ and the absolute net charge proved the most interesting to consider. Replotting the data from Figure 3 as a function of the net charge of the protein highlights the dramatically different behaviour of HEWL, compared with BSA and Hb (Figure 8a,b). Additionally, Figure S19a,b demonstrates that HEWL has a significantly higher number of charges per residue than the other two proteins. However, we hypothesize that the significantly higher encapsulation efficiency and partitioning of HEWL is not merely due to the higher charge density, but is a result of the charge patch identified in Figure 6c. Thus, if we consider the trends for BSA and Hb separately, we observe a slow increase in uptake with increasing protein charge for cases where charge is distributed uniformly across the protein surface, while dramatic increases are observed when a charge patch is present.

If we consider the relative distance from the isoelectric point $|pI - pH|$ (Figure 8c,d), we observed similar trends. In particular, these results suggest the possibility of different scaling behaviour for the case of proteins with uniform charge and those with a charge patch (see dashed lines in Figure 8d). Although true validation of such trends will require consideration of a much larger number of proteins, we suggest that the relatively slow rate of increase in protein incorporation with changing pH might be a general phenomenon for proteins with relatively isotropic distributions of surface charge, while the sharper rate of increase observed for HEWL might be characteristic of proteins with distinct charge patches. Furthermore, we hypothesize that it is the observed rate of change that may serve as a descriptor for the system, rather than encapsulation at a specific value of $|pI - pH|$. However, because of the relatively small number of samples and conditions explored in this current work, it is possible that the observed trends in our data are simply fortuitous. Thus, it will be interesting to see whether such trends in protein uptake occur for other protein systems.

In a small step towards a broader exploration of additional protein systems, we plotted preliminary data for the incorporation of a novel monoclonal antibody (mAb) into our K_{50}/E_{50} coacervates at pH 6.0, ($pI = 8.8$). The experimentally determined values for both encapsulation efficiency and partition coefficient fall into a similar range as our previous data (black diamonds, Figure 8c,d). While the structure of this antibody is not known, mAbs typically have patches of both positive and negative residues. Thus, it is unclear how the uptake of such a protein would compare to the other potential classes described here, beyond the apparent agreement of one data point.

Whether simple metrics such as net charge or distance from the isoelectric point ultimately prove to have some predictive utility or not, one important takeaway from our results is the potential for two-polymer coacervates to enable the effective encapsulation of proteins with very low net charge (*e.g.*, Hb at pH = 8.0 has a ratio of positive-to-negative charges close to 1.0), which would not be predicted to form coacervates in a binary system.[8]

Conclusions

In summary, we have explored the potential for using a two-polymer coacervate system to effectively encapsulate a variety of model proteins across a range of solution conditions and polymer properties. While electrostatic considerations such as salt concentration and solution pH are critical in the design of an encapsulation strategy, the use of a two-polymer coacervate system can provide the flexibility to encapsulate even weakly-charged proteins near their isoelectric point.

We also highlighted the importance of the charge density of the polymer and the presence of charge patches on the protein on the resulting encapsulation. With respect to the distribution of charge on the protein surface, our results suggest possible different scaling behaviours for proteins with isotropic vs. patchy distributions of charges, as a function of either net charge or the relative distance from the isoelectric point $|pI - pH|$. Our results also suggested the potential for using sequence-defined polymers to enhance protein encapsulation and/or potentially enable the selective uptake of one protein species over another. However, further investigations are needed to elucidate details and determine whether the promising trends observed here can be translated into predictive tools to effectively design encapsulation strategies for novel targets.

Conflicts of interest

There are no conflicts to declare.

Acknowledgements

We acknowledge MassBiologics of University of Massachusetts Medical School for the gift of the monoclonal antibody. We would like to thank the University of Massachusetts Amherst Armstrong Fund for Science and Soft Materials for Life Sciences National Research Training grant from the National Science Foundation (NRT# 1545399) for support. We also would like to thank L.W. Chang for help with polypeptide synthesis and K. Rahlwes, M.D. Langer, and C.E. Sing for helpful discussions.

References

(1) Pisal, D. S.; Kosloski, M. P.; Balu-Iyer, S. V. Delivery of therapeutic proteins. *J. Pharm. Sci.* **2010**, *99* (6), 2557–2575 DOI: 10.1002/jps.22054.

(2) Perry, S.; Li, Y.; Priftis, D.; Leon, L.; Tirrell, M. The effect of salt on the complex coacervation of vinyl polyelectrolytes. *Polymers* **2014**, *6* (6), 1756–1772 DOI: 10.3390/polym6061756.

(3) Priftis, D.; Leon, L.; Song, Z.; Perry, S. L.; Margossian, K. O.; Tropnikova, A.; Cheng, J.; Tirrell, M. Self-assembly of α-helical polypeptides driven by complex coacervation. *Angew. Chem. Int. Ed.* **2015**, *127* (38), 11280–11284 DOI: 10.1002/ange.201504861.

(4) Hoffmann, K. Q.; Perry, S. L.; Leon, L.; Priftis, D.; Tirrell, M.; de Pablo, J. J. A molecular view of the role of chirality in charge-driven polypeptide complexation. *Soft Matter* **2015**, *11* (8), 1525–1538 DOI: 10.1039/C4SM02336F.

(5) Water, J. J.; Schack, M. M.; Velazquez-Campoy, A.; Maltesen, M. J.; van de Weert, M.; Jorgensen, L. Complex coacervates of hyaluronic acid and lysozyme: Effect on protein structure and physical stability. *Eur. J. Pharm. Biopharm.* **2014**, *88* (2), 325–331 DOI: 10.1016/j.ejpb.2014.09.001.

(6) Perry, S. L.; Leon, L.; Hoffmann, K. Q.; Kade, M. J.; Priftis, D.; Black, K. A.; Wong, D.; Klein, R. A.; Pierce, C. F.; Margossian, K. O.; et al. Chirality-selected phase behaviour in ionic polypeptide complexes. *Nat. Commun.* **2015**, *6* (1), 6052 DOI: 10.1038/ncomms7052.

(7) Black, K. A.; Priftis, D.; Perry, S. L.; Yip, J.; Byun, W. Y.; Tirrell, M. Protein encapsulation via polypeptide complex coacervation. *ACS Macro Lett.* **2014**, *3* (10), 1088–1091 DOI: 10.1021/mz500529v.

(8) Obermeyer, A. C.; Mills, C. E.; Dong, X.-H.; Flores, R. J.; Olsen, B. D. Complex coacervation of supercharged proteins with polyelectrolytes. *Soft Matter* **2016**, *12*, 3570–3581 DOI: 10.1039/C6SM00002A.

(9) Pippa, N.; Karayianni, M.; Pispas, S.; Demetzos, C. Complexation of cationic-neutral block polyelectrolyte with insulin and in vitro release studies. *Int. J. Pharm.* **2015**, *491* (1-2), 136–143 DOI: 10.1016/j.ijpharm.2015.06.013.

(10) Pippa, N.; Kalinova, R.; Dimitrov, I.; Pispas, S.; Demetzos, C. Insulin/poly(ethylene glycol)- block-poly(l-lysine) Complexes: Physicochemical Properties and Protein Encapsulation. *J. Phys. Chem. B* **2015**, *119* (22), 6813–6819 DOI: 10.1021/acs.jpcb.5b01664.

(11) Nolles, A.; Westphal, A. H.; de Hoop, J. A.; Fokkink, R. G.; Kleijn, J. M.; van Berkel, W. J. H.; Borst, J. W.; Westphal, A. H. Encapsulation of GFP in complex coacervate core micelles. *Biomacromolecules* **2015**, *16* (5), 1542–1549 DOI: 10.1021/acs.biomac.5b00092.

(12) Chen, W. C. W.; Lee, B. G.; Park, D. W.; Kim, K.; Chu, H.; Kim, K.; Huard, J.; Wang, Y. Controlled dual delivery of fibroblast growth factor-2 and Interleukin-10 by heparin-based coacervate synergistically enhances ischemic heart repair. *Biomaterials* **2015**, *72* (c), 138–151 DOI: 10.1016/j.biomaterials.2015.08.050.

(13) Kim, S.; Huang, J.; Lee, Y.; Dutta, S.; Yoo, H. Y.; Jung, Y. M.; Jho, Y.; Zeng, H.; Hwang, D. S. Complexation and coacervation of like-charged polyelectrolytes inspired by mussels. *Proc. Natl. Acad. Sci. U.S.A.* **2016**, *113* (7), E847–E853 DOI: 10.1073/pnas.1521521113.

(14) Kawamura, A.; Harada, A.; Kono, K.; Kataoka, K. Self-Assembled Nano-Bioreactor from Block Ionomers with Elevated and Stabilized Enzymatic Function. *Bioconjugate Chem.* **2007**, *18* (5), 1555–1559 DOI: 10.1021/bc070029t.

(15) Jaturanpinyo, M.; Harada, A.; Yuan, X.; Kataoka, K. Preparation of Bionanoreactor Based on Core−Shell Structured Polyion Complex Micelles Entrapping Trypsin in the Core Cross-Linked with Glutaraldehyde. *Bioconjugate Chem.* **2004**, *15* (2), 344–348 DOI: 10.1021/bc034149m.

(16) Harada, A.; Kataoka, K. Pronounced activity of enzymes through the incorporation into the core of polyion complex micelles made from charged block copolymers. *J. Controlled Release* **2001**, *72*, 85–91.

(17) Kataoka, K.; Harada, A.; Nagasaki, Y. Block copolymer micelles for drug delivery: design, characterization and biological significance. *Adv. Drug Delivery Rev.* **2001**, *47*, 113–131.

(18) Harada, A.; Kataoka, K. Novel Polyion Complex Micelles Entrapping Enzyme Molecules in the Core. 2. Characterization of the Micelles Prepared at Nonstoichiometric Mixing Ratios. *Langmuir* **1999**, *15* (12), 4208–4212 DOI: 10.1021/la981087t.

(19) Harada, A.; Kataoka, K. Novel Polyion Complex Micelles Entrapping Enzyme Molecules in the Core: Preparation of Narrowly-Distributed Micelles from Lysozyme and Poly(ethylene glycol)-Poly(aspartic acid) Block Copolymer in Aqueous Medium. *Macromolecules* **1998**, *31*, 288–294.

(20) Harada, A.; Kataoka, K. Formation of Polyion Complex Micelles in an Aqueous Milieu from a Pair of Oppositely-Charged Block Copolymers with Poly(ethylene glycol) Segments. *Macromolecules* **1995**, *28*, 5294–5299.

(21) Voets, I. K.; de Keizer, A.; Cohen Stuart, M. A. Complex coacervate core micelles. *Adv. Colloid Interface Sci.* **2009**, *147-148* (C), 300–318 DOI: 10.1016/j.cis.2008.09.012.

(22) Kayitmazer, A. B.; Seyrek, E.; Dubin, P. L.; Staggemeier, B. A. Influence of Chain Stiffness on the Interaction of Polyelectrolytes with Oppositely Charged Micelles and Proteins. *J. Phys. Chem. B* **2003**, *107* (32), 8158–8165 DOI: 10.1021/jp034065a.

(23) Kalantar, T. H.; Tucker, C. J.; Zalusky, A. S.; Boomgaard, T. A.; Wilson, B. E.; Ladika, M.; Jordan, S. L.; Li, W. K.; Zhang, X.; Goh, C. G. High throughput workflow for coacervate formation and characterization in shampoo systems. *J. Cosmet. Sci.* **2007**, *58*, 375–383.

(24) Hu, D.; Chou, K. C. Re-evaluating the surface tension analysis of polyelectrolyte-surfactant mixtures using phase-sensitive

sum frequency generation spectroscopy. *J. Am. Chem. Soc.* **2014**, *136* (43), 15114–15117 DOI: 10.1021/ja5049175.

(25) Nejati, M. M.; Khaledi, M. G. Perfluoro-alcohol-induced complex coacervates of polyelectrolyte–surfactant mixtures: Phase behavior and analysis. *Langmuir* **2015**, *31* (20), 5580–5589 DOI: 10.1021/acs.langmuir.5b00444.

(26) Szczepanowicz, K.; Bazylińska, U.; Pietkiewicz, J.; Szyk-Warszyńska, L.; Wilk, K. A.; Warszyński, P. Biocompatible long-sustained release oil-core polyelectrolyte nanocarriers: From controlling physical state and stability to biological impact. *Adv. Colloid Interface Sci.* **2015**, *222* (C), 678–691 DOI: 10.1016/j.cis.2014.10.005.

(27) Wang, Y.; Kimura, K.; Huang, Q.; Dubin, P. L.; Jaeger, W. Effects of Salt on Polyelectrolyte−Micelle Coacervation. *Macromolecules* **1999**, *32* (21), 7128–7134 DOI: 10.1021/ma990972v.

(28) Wang, W.; Mauroy, H.; Zhu, K.; Knudsen, K. D.; Kjøniksen, A.-L.; Nyström, B.; Sande, S. A. Complex coacervate micelles formed by a C18-capped cationic triblock thermoresponsive copolymer interacting with SDS. *Soft Matter* **2012**, *8* (45), 11514–11525 DOI: 10.1039/c2sm26567b.

(29) Kizilay, E.; Kayitmazer, A. B.; Dubin, P. L. Complexation and coacervation of polyelectrolytes with oppositely charged colloids. *Adv. Colloid Interface Sci.* **2011**, *167* (1-2), 24–37 DOI: 10.1016/j.cis.2011.06.006.

(30) Schmitt, C.; Turgeon, S. L. Protein/polysaccharide complexes and coacervates in food systems. *Adv. Colloid Interface Sci.* **2011**, *167* (1-2), 63–70 DOI: 10.1016/j.cis.2010.10.001.

(31) Yeo, Y.; Bellas, E.; Firestone, W.; Langer, R.; Kohane, D. S. Complex Coacervates for Thermally Sensitive Controlled Release of Flavor Compounds. *J. Agric. Food Chem.* **2005**, *53* (19), 7518–7525 DOI: 10.1021/jf0507947.

(32) Carvalho, I. T.; Estevinho, B. N.; Santos, L. Application of microencapsulated essential oils in cosmetic and personal healthcare products - A review. *Int. J. Cosmet. Sci.* **2016**, *38* (2), 109–119 DOI: 10.1111/ics.12232.

(33) Martins, I. M.; Barreiro, M. F.; Coelho, M.; Rodrigues, A. E. Microencapsulation of essential oils with biodegradable polymeric carriers for cosmetic applications. *Chem. Eng. J.* **2014**, *245* (C), 191–200 DOI: 10.1016/j.cej.2014.02.024.

(34) Kuo, C.-H.; Leon, L.; Chung, E. J.; Huang, R.-T.; Sontag, T. J.; Reardon, C. A.; Getz, G. S.; Tirrell, M.; Fang, Y. Inhibition of atherosclerosis-promoting microRNAs via targeted polyelectrolyte complex micelles. *J. Mater. Chem. B* **2014**, *2*, 8142–8153 DOI: 10.1039/C4TB00977K.

(35) Kishimura, A.; Koide, A.; Osada, K.; Yamasaki, Y.; Kataoka, K. Encapsulation of Myoglobin in PEGylated Polyion Complex Vesicles Made from a Pair of Oppositely Charged Block Ionomers: A Physiologically Available Oxygen Carrier. *Angew. Chem. Int. Ed.* **2007**, *46* (32), 6085–6088 DOI: 10.1002/anie.200701776.

(36) Vehlow, D.; Schmidt, R.; Gebert, A.; Siebert, M.; Lips, K.; Müller, M. Polyelectrolyte complex based interfacial drug delivery system with controlled loading and improved release performance for bone therapeutics. *Nanomaterials* **2016**, *6* (3), 53–21 DOI: 10.3390/nano6030053.

(37) Cummings, C. S.; Obermeyer, A. C. Phase Separation Behavior of Supercharged Proteins and Polyelectrolytes. *Biochemistry* **2018**, *57* (3), 314–323 DOI: 10.1021/acs.biochem.7b00990.

(38) Kapelner, R. A.; Obermeyer, A. C. Ionic polypeptide tags for protein phase separation. *Chem. Sci.* **2019**, *9* (4), e1442–e1448 DOI: 10.1039/C8SC04253E.

(39) Priftis, D.; Xia, X.; Margossian, K. O.; Perry, S. L.; Leon, L.; Qin, J.; de Pablo, J. J.; Tirrell, M. Ternary, tunable polyelectrolyte complex fluids driven by complex coacervation. *Macromolecules* **2014**, *47* (9), 3076–3085 DOI: 10.1021/ma500245j.

(40) Brangwynne, C. P.; Mitchison, T. J.; Hyman, A. A. Active liquid-like behavior of nucleoli determines their size and shape in Xenopus laevis oocytes. *Proc. Natl. Acad. Sci. U.S.A.* **2011**, *108* (11), 4334–4339 DOI: 10.1073/pnas.1017150108.

(41) Hyman, A. A.; Simons, K. Beyond Oil and Water--Phase Transitions in Cells. *Science* **2012**, *337* (6098), 1047–1049 DOI: 10.1126/science.1223728.

(42) Weber, S. C.; Brangwynne, C. P. Getting RNA and Protein in Phase. *Cell* **2012**, *149* (6), 1188–1191 DOI: 10.1016/j.cell.2012.05.022.

(43) Weber, S. C. Sequence-encoded material properties dictate the structure and function of nuclear bodies. *Curr. Opin. Cell Biol.* **2017**, *46*, 62–71 DOI: 10.1016/j.ceb.2017.03.003.

(44) Hyman, A. A.; Weber, C. A.; Jülicher, F. Liquid-Liquid Phase Separation in Biology. *Annu. Rev. Cell Dev. Biol.* **2014**, *30* (1), 39–58 DOI: 10.1146/annurev-cellbio-100913-013325.

(45) Brangwynne, C. P.; Tompa, P.; Pappu, R. V. Polymer physics of intracellular phase transitions. *Nat. Phys.* **2015**, *11* (11), 899–904 DOI: 10.1038/nphys3532.

(46) Banani, S. F.; Lee, H. O.; Hyman, A. A.; Rosen, M. K. Biomolecular condensates: organizers of cellular biochemistry. *Nat. Rev. Mol. Cell Biol.* **2017**, *18* (5), 285–298 DOI: 10.1038/nrm.2017.7.

(47) Zhu, L.; Brangwynne, C. P. Nuclear bodies: the emerging biophysics of nucleoplasmic phases. *Curr. Opin. Cell Biol.* **2015**, *34*, 23–30 DOI: 10.1016/j.ceb.2015.04.003.

(48) Martin, E. W.; Mittag, T. Relationship of Sequence and Phase Separation in Protein Low-Complexity Regions. *Biochemistry* **2018**, *57* (17), 2478–2487 DOI: 10.1021/acs.biochem.8b00008.

(49) Bayas, C. A.; Wang, J.; Lee, M. K.; Schrader, J. M.; Shapiro, L.; Moerner, W. E. Spatial organization and dynamics of RNase E and ribosomes in Caulobacter crescentus. *Proc. Natl. Acad. Sci. U.S.A.* **2018**, *115* (16), E3712–E3721 DOI: 10.1073/pnas.1721648115.

(50) Werner, J. N.; Chen, E. Y.; Guberman, J. M.; Zippilli, A. R.; Irgon, J. J.; Gitai, Z. Quantitative genome-scale analysis of protein localization in an asymmetric bacterium. *Proc. Natl. Acad. Sci. U.S.A.* **2009**, *106* (19), 7858–7863.

(51) Perry, S. L. Phase Separation: Bridging Polymer Physics and Biology. *Curr. Opin. Colloid Interface Sci.* **2019**, *39*, 86–97 DOI: 10.1016/j.cocis.2019.01.007.

(52) Nott, T. J.; Craggs, T. D.; Baldwin, A. J. Membraneless organelles can melt nucleic acid duplexes and act as biomolecular filters. *Nat. Chem.* **2016**, *8* (6), 569–575 DOI: 10.1038/nchem.2519.

(53) Nott, T. J.; Petsalaki, E.; Farber, P.; Jervis, D.; Fussner, E.; Plochowietz, A.; Craggs, T. D.; Bazett-Jones, D. P.; Pawson, T.; Forman-Kay, J. D.; et al. Phase transition of a disordered nuage protein generates environmentally responsive membraneless organelles. *Mol. Cell* **2015**, *57* (5), 936–947 DOI: 10.1016/j.molcel.2015.01.013.

(54) Pak, C. W.; Kosno, M.; Holehouse, A. S.; Padrick, S. B.; Mittal, A.; Ali, R.; Yunus, A. A.; Liu, D. R.; Pappu, R. V.; Rosen, M. K. Sequence determinants of intracellular phase separation by complex coacervation of a disordered protein. *Mol. Cell*

2016, *63* (1), 72–85 DOI: 10.1016/j.molcel.2016.05.042.
(55) Narayanaswamy, R.; Levy, M.; Tsechansky, M.; Stovall, G. M.; O'Connell, J. D.; Mirrielees, J.; Ellington, A. D.; Marcotte, E. M. Widespread reorganization of metabolic enzymes into reversible assemblies upon nutrient starvation. *Proc. Natl. Acad. Sci. U.S.A.* **2009**, *106* (25), 10147–10152 DOI: 10.1073/pnas.0812771106.
(56) An, S.; Kumar, R.; Sheets, E. D.; Benkovic, S. J. Reversible Compartmentalization of de Novo Purine Biosynthetic Complexes in Living Cells. *Science* **2008**, *320* (5872), 103–106 DOI: 10.1126/science.1152241.
(57) Wippich, F.; Bodenmiller, B.; Trajkovska, M. G.; Wanka, S.; Aebersold, R.; Pelkmans, L. Dual Specificity Kinase DYRK3 Couples Stress Granule Condensation/Dissolution to mTORC1 Signaling. *Cell* **2013**, *152* (4), 791–805 DOI: 10.1016/j.cell.2013.01.033.
(58) Berry, J.; Brangwynne, C. P.; Haataja, M. Physical principles of intracellular organization via active and passive phase transitions. *Rep. Prog. Phys.* **2018**, *81* (4), 046601–046643 DOI: 10.1088/1361-6633/aaa61e.
(59) Malinovska, L.; Kroschwald, S.; Alberti, S. Protein disorder, prion propensities, and self-organizing macromolecular collectives. *BBA - Proteins and Proteomics* **2013**, *1834* (5), 918–931 DOI: 10.1016/j.bbapap.2013.01.003.
(60) Molliex, A.; Temirov, J.; Lee, J.; Coughlin, M.; Kanagaraj, A. P.; Kim, H. J.; Mittag, T.; Taylor, J. P. Phase Separation by Low Complexity Domains Promotes Stress Granule Assembly and Drives Pathological Fibrillization. *Cell* **2015**, *163* (1), 123–133 DOI: 10.1016/j.cell.2015.09.015.
(61) Uversky, V. N. Protein intrinsic disorder-based liquid-liquid phase transitions in biological systems: Complex coacervates and membrane-less organelles. *Adv. Colloid Interface Sci.* **2017**, *239* (C), 97–114 DOI: 10.1016/j.cis.2016.05.012.
(62) Tang, H.; Sakamura, Y.; Mori, T.; Katayama, Y.; Kishimura, A. Development of Enzyme Loaded Polyion Complex Vesicle (PICsome): Thermal Stability of Enzyme in PICsome Compartment and Effect of Coencapsulation of Dextran on Enzyme Activity. *Macromol. Biosci.* **2017**, *5*, 1600542–1600547 DOI: 10.1002/mabi.201600542.
(63) Amblard, M.; Fehrentz, J.-A.; Martinez, J.; Subra, G. Methods and Protocols of Modern Solid Phase Peptide Synthesis. *Mol. Biotechnol.* **2006**, *33* (3), 239–254 DOI: 10.1385/MB:33:3:239.
(64) Pacalin, N. M.; Leon, L.; Tirrell, M. Directing the phase behavior of polyelectrolyte complexes using chiral patterned peptides. *Eur. Phys. J. Spec. Top.* **2016**, *225* (8-9), 1805–1815 DOI: 10.1140/epjst/e2016-60149-6.
(65) Chang, L.-W.; Lytle, T. K.; Radhakrishna, M.; Madinya, J. J.; Vélez, J.; Sing, C. E.; Perry, S. L. Sequence and entropy-based control of complex coacervates. *Nat. Commun.* **2017**, 1–7 DOI: 10.1038/s41467-017-01249-1.
(66) Wendorf, J. R.; Radke, C. J.; Blanch, H. W. The role of electrolytes on protein adsorption at a hydrophilic solid–water interface. *Colloids Surf., B* **2010**, *75*, 100–106 DOI: 10.1016/j.colsurfb.2009.08.015.
(67) Ang, W. S.; Elimelech, M. Protein (BSA) fouling of reverse osmosis membranes: Implications for wastewater reclamation. *J. Membr. Sci.* **2007**, *296* (1-2), 83–92 DOI: 10.1016/j.memsci.2007.03.018.
(68) Shi, Q.; Zhou, Y.; Sun, Y. Influence of pH and Ionic Strength on the Steric Mass-Action Model Parameters around the Isoelectric Point of Protein. *Biotechnol. Prog.* **2005**, *21* (2), 516–523 DOI: 10.1021/bp049735o.
(69) Cho, D.; Narsimhan, G.; Franses, E. I. Adsorption Dynamics of Native and Alkylated Derivatives of Bovine Serum Albumin at Air–Water Interfaces. *J. Colloid Interface Sci.* **1996**, *178* (123), 348–357 DOI: 10.1006/jcis.1996.0123.
(70) Nguyen, T. T.-B.; Chang, H.-C.; Wu, V. W.-K. Adsorption and hydrolytic activity of lysozyme on diamond nanocrystallites. *Diamond Relat. Mater.* **2007**, *16* (4-7), 872–876 DOI: 10.1016/j.diamond.2007.01.030.
(71) Koepke, J. A.; Miller, L. Fractionation of Human Hemoglobins Using Isoelectric Focusing. *Ann. Clin. Lab. Sci.* **1972**, *2* (4), 335–342.
(72) Koepke, J. A.; Thoma, J. F.; Schmidt, R. M. Identification of Human Hemoglobins by Use of Isoelectric Focusing in Gel. *Clin. Chem.* **1975**, *21* (13), 1953–1955.
(73) Ui, N. Isolectric Points and Conformation of Proteins. *Biochim. Biophys. Acta* **1971**, *229*, 567–581.
(74) Pauling, L.; Itano, H. A.; Singer, S. J.; Wells, I. C. Sickle Cell Anemia, a Molecular Disease. *Science* **1949**, *110* (2865), 543–548.
(75) Berman, H. M.; Westbrook, J.; Feng, Z.; Gilliland, G.; Bhat, T. N.; Weissig, H.; Shindyalov, I. N.; Bourbe, P. E. Protein Data Bank. *Nucleic Acids Res. 28*, 235–242.
(76) Majorek, K. A.; Porebski, P. J.; Dayal, A.; Zimmerman, M. D.; Jablonska, K.; Stewart, A. J.; Chruszcz, M.; Minor, W. Structural and immunologic characterization of bovine, horse, and rabbit serum albumins. *Mol. Immunol.* **2012**, *52* (3-4), 174–182 DOI: 10.1016/j.molimm.2012.05.011.
(77) Park, S.-Y.; Yokoyama, T.; Shibayama, N.; Shiro, Y.; Tame, J. R. H. 1.25 Å Resolution Crystal Structures of Human Haemoglobin in the Oxy, Deoxy and Carbonmonoxy Forms. *J. Mol. Biol.* **2006**, *360* (3), 690–701 DOI: 10.1016/j.jmb.2006.05.036.
(78) Weiss, M. S.; Palm, G. J.; Hilgenfeld, R. Crystallization, structure solution and refinement of hen egg-white lysozyme at pH 8.0 in the presence of MPD. *Acta Crystallogr. D Biol. Crystallogr.* **2000**, *56* (Pt 8), 952–958.
(79) Comert, F.; Malanowski, A. J.; Azarikia, F.; Dubin, P. L. Coacervation and precipitation in polysaccharide-protein systems. *Soft Matter* **2016**, *12*, 4154–4161 DOI: 10.1039/C6SM00044D.
(80) Priftis, D.; Tirrell, M. Phase behaviour and complex coacervation of aqueous polypeptide solutions. *Soft Matter* **2012**, *8* (36), 9396–9405 DOI: 10.1039/C2SM25604E.
(81) Tal, M.; Silberstein, A.; Nusser, E. Why Does Coomassie Brilliant Blue R Interact Differently with Different Proteins? *J. Biol. Chem.* **1985**, *260* (18), 9976–9980.
(82) Blocher, W. C.; Perry, S. L. Complex coacervate-based materials for biomedicine. *WIREs Nanomed. Nanobiotechnol.* **2017**, *9* (4), e1442–28 DOI: 10.1002/wnan.1442.
(83) Flanagan, S. E.; Malanowski, A. J.; Kizilay, E.; Seeman, D.; Dubin, P. L.; Donato-Capel, L.; Bovetto, L.; Schmitt, C. Complex equilibria, speciation, and heteroprotein coacervation of lactoferrin and β-lactoglobulin. *Langmuir* **2015**, *31* (5), 1776–1783 DOI: 10.1021/la504020e.
(84) Huang, S.; Zhao, M.; Dawadi, M. B.; Cai, Y.; Lapitsky, Y.; Modarelli, D. A.; Zacharia, N. S. Effect of small molecules on the phase behavior and coacervation of aqueous solutions of poly(diallyldimethylammonium chloride) and poly(sodium 4-styrene sulfonate). *J. Colloid Interface Sci.* **2018**, *518*, 216–224 DOI: 10.1016/j.jcis.2018.02.029.

(85) Lindhoud, S.; Claessens, M. M. A. E. Accumulation of small protein molecules in a macroscopic complex coacervate. *Soft Matter* **2015**, *12* (2), 408–413 DOI: 10.1039/C5SM02386F.

(86) Lindhoud, S.; de Vries, R.; Schweins, R.; Cohen Stuart, M. A.; Norde, W. Salt-induced release of lipase from polyelectrolyte complex micelles. *Soft Matter* **2009**, *5* (1), 242–250 DOI: 10.1039/B811640G.

(87) Peng, B.; Muthukumar, M. Modeling competitive substitution in a polyelectrolyte complex. *J. Chem. Phys.* **2015**, *143* (24), 243133–11 DOI: 10.1063/1.4936256.

(88) Wang, Q.; Schlenoff, J. B. The polyelectrolyte complex/coacervate continuum. *Macromolecules* **2014**, *47* (9), 3108–3116 DOI: 10.1021/ma500500q.

(89) Spruijt, E.; Westphal, A. H.; Borst, J. W.; Cohen Stuart, M. A.; van der Gucht, J. Binodal Compositions of Polyelectrolyte Complexes. *Macromolecules* **2010**, *43* (15), 6476–6484 DOI: 10.1021/ma101031t.

(90) Li, L.; Srivastava, S.; Andreev, M.; Marciel, A. B.; de Pablo, J. J.; Tirrell, M. V. Phase Behavior and Salt Partitioning in Polyelectrolyte Complex Coacervates. *Macromolecules* **2018**, *51* (8), 2988–2995 DOI: 10.1021/acs.macromol.8b00238.

(91) Sadman, K.; Wang, Q.; Chen, Y.; Keshavarz, B.; Jiang, Z.; Shull, K. R. Influence of Hydrophobicity on Polyelectrolyte Complexation. *Macromolecules* **2017**, *50* (23), 9417–9426 DOI: 10.1021/acs.macromol.7b02031.

(92) Ghostine, R. A.; Shamoun, R. F.; Schlenoff, J. B. Doping and Diffusion in an Extruded Saloplastic Polyelectrolyte Complex. *Macromolecules* **2013**, *46* (10), 4089–4094 DOI: 10.1021/ma4004083.

(93) O'Neal, J. T.; Wilcox, K. G.; Zhang, Y.; George, I. M.; Lutkenhaus, J. L. Comparison of KBr and NaCl effects on the glass transition temperature of hydrated layer-by-layer assemblies. *J. Chem. Phys.* **2018**, *149* (16), 163317–163317 DOI: 10.1063/1.5037491.

(94) O'Neal, J. T.; Dai, E. Y.; Zhang, Y.; Clark, K. B.; Wilcox, K. G.; George, I. M.; Ramasamy, N. E.; Enriquez, D.; Batys, P.; Sammalkorpi, M.; et al. QCM-D Investigation of Swelling Behavior of Layer-by-Layer Thin Films upon Exposure to Monovalent Ions. *Langmuir* **2018**, *34* (3), 999–1009 DOI: 10.1021/acs.langmuir.7b02836.

(95) Saurabh, S.; Sahoo, P. K. Lysozyme: an important defence molecule of fish innate immune system. *Aquaculture Res.* **2008**, *39* (3), 223–239 DOI: 10.1111/j.1365-2109.2007.01883.x.

(96) Ragland, S. A.; Criss, A. K. From bacterial killing to immune modulation: Recent insights into the functions of lysozyme. *PLoS Pathog.* **2017**, *13* (9), e1006512–e1006522 DOI: 10.1371/journal.ppat.1006512.

(97) Ibrahim, H. R.; Matsuzaki, T.; Aoki, T. Genetic evidence that antibacterial activity of lysozyme is independent of its catalytic function. *FEBS Lett.* **2001**, *506*, 27–32.

(98) Xu, Y.; Mazzawi, M.; Chen, K.; Sun, L.; Dubin, P. L. Protein Purification by Polyelectrolyte Coacervation: Influence of Protein Charge Anisotropy on Selectivity. *Biomacromolecules* **2011**, *12* (5), 1512–1522 DOI: 10.1021/bm101465y.

Design Rules for Encapsulating Proteins into Complex Coacervates Supplemental Information

Whitney C. Blocher McTigue and Sarah L. Perry*
Department of Chemical Engineering, University of Massachusetts Amherst
*Correspondence: perrys@engin.umass.edu

TOC Figure:

We explore using two-polymer coacervation to encapsulate model proteins and present design rules to guide encapsulation of novel targets.